Chapter 5
The Large Scale Ocean Circulation and Physical Processes Controlling Pacific-Arctic Interactions

Wieslaw Maslowski, Jaclyn Clement Kinney, Stephen R. Okkonen, Robert Osinski, Andrew F. Roberts, and William J. Williams

Abstract Understanding oceanic effects on climate in the Pacific-Arctic region requires knowledge of the mean circulation and its variability in the region. This chapter presents an overview of the mean regional circulation patterns, spatial and temporal variability, critical processes and property fluxes from the northern North Pacific into the western Arctic Ocean, with emphasis on their impact on sea ice. First, results from a high-resolution, pan-Arctic ice-ocean model forced with realistic atmospheric data and observations in the Alaskan Stream, as well as exchanges across the Aleutian Island Passes, are discussed. Next, general ocean circulation in the deep Bering Sea, shelf-basin exchange, and flow across the Bering shelf are investigated. Also, flow across the Chukchi Sea, pathways of Pacific summer water and oceanic forcing of sea ice in the Pacific-Arctic region are analyzed. Finally, we hypothesize that the northward advection of Pacific Water together with the excess oceanic heat that has accumulated below the surface mixed layer in the western Arctic Ocean due to diminishing sea ice cover and subsequent increased solar insolation are critical factors affecting sea ice growth in winter and melt the following year.

W. Maslowski (✉) • J. Clement Kinney
Department of Oceanography, Graduate School of Engineering and Applied Sciences, Naval Postgraduate School, Dyer Road, Bldg. SP339B, Monterey, CA 93943, USA
e-mail: maslowsk@nps.edu; jlclemen@nps.edu

S.R. Okkonen
School of Fisheries and Ocean Sciences, University of Alaska, Fairbanks, AK 99775, USA

R. Osinski
Institute of Oceanology, Polish Academy of Sciences, Powstancow Warszawy 55, Sopot 81-712, Poland

A.F. Roberts
Department of Oceanography, Naval Postgraduate School, Dyer Road, Bldg. SP339B, Monterey, CA 93943, USA

W.J. Williams
Fisheries and Oceans Canada, Institute of Ocean Sciences, Sidney, BC, Canada V8L 4B2
e-mail: Bill.Williams@dfo-mpo.gc.ca

We argue that process-level understanding and improved model representation of ocean dynamics and ocean-ice-atmosphere interactions in the Pacific-Arctic region are needed to advance knowledge and improve prediction of the accelerated decline of sea ice cover and amplified climate warming in the Arctic.

Keywords Ocean circulation • Alaskan Stream • Bering Sea • Western Arctic • Ice-ocean modeling

5.1   Introduction

This chapter focuses on the physical oceanography of the Pacific-Arctic Region (PAR). For our purposes, PAR is defined to include the Gulf of Alaska, northern North Pacific, and the Bering, Chukchi, Beaufort, and East Siberian seas. Figure 5.1
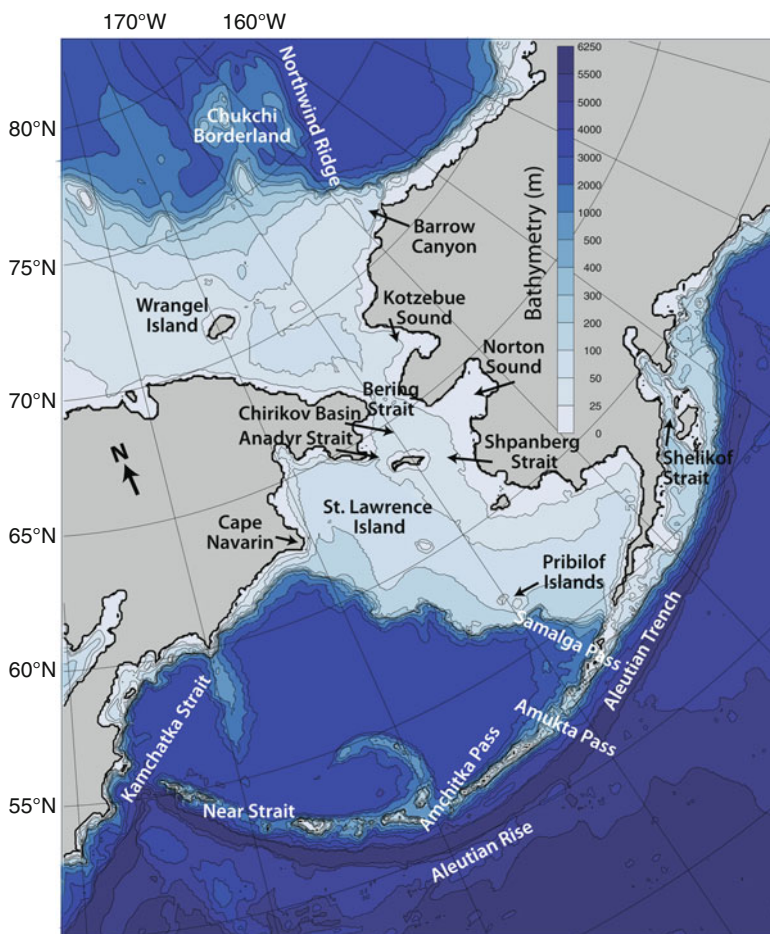

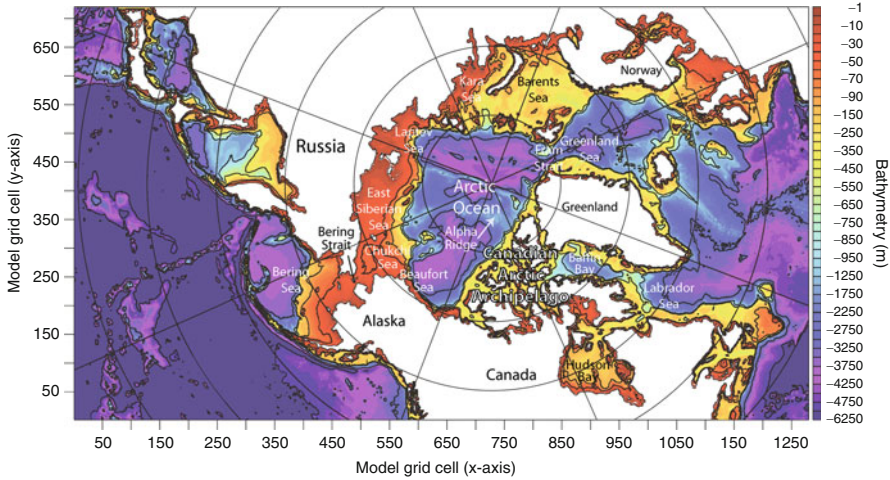**Fig. 5.1** Bathymetry (m) of the Pacific-Arctic Region

Fig. 5.2 The NAME model domain and bathymetry (m)

shows the bathymetry and geographic place names for the PAR region. To our knowledge, there has been no recent physical oceanography review of this region. Stabeno et al. (1999) reviewed the physical oceanography of the Bering Sea and described observational results on the flow through the Aleutian Island Passes and the general circulation throughout the Bering Sea. They stated a need for more information on: (1) the transport variability and magnitude of the flow through the Aleutian Island Passes, (2) deep Bering Sea circulation, and (3) mechanisms that provide nutrients to the euphotic zone along the Bering Slope. Results presented in this chapter and in Chap. 6 by Williams et al. (2014, this volume) provide more information in these three areas.

Along with observational results from several authors, we will discuss results from the Naval Postgraduate School (NPS) Arctic Modeling Effort (NAME) coupled sea ice-ocean model in this chapter. The model has a horizontal grid spacing of 1/12° (or ~9 km) and 45 vertical depth layers. At this horizontal resolution the model is considered eddy permitting, as mesoscale features down to ~37 km in diameter (four grid points) can be resolved (Maslowski et al. 2008b). In the vertical direction, eight levels are in the upper 50 m and 15 levels in the upper 200 m. The high vertical resolution, especially in the upper water column, allows for more realistic representation of the shallow Arctic and sub-Arctic shelves than a lower vertical resolution typical in many ocean models. The model domain contains the sub-Arctic North Pacific and North Atlantic Oceans, the Arctic Ocean, the Canadian Arctic Archipelago (CAA) and the Nordic Seas (Fig. 5.2). The choice of model domain was in part dictated by the need for realistic prediction of the net northward transport of water mass and properties through Bering Strait and consequently the circulation and variability in volume and heat fluxes entering the Beaufort Sea from the Chukchi Shelf. Additional details of this model are discussed by Clement Kinney et al. (2014, this volume), Maslowski et al. (2004) and Maslowski et al. (2008a, b).

5.2   The Northern North Pacific, Gulf of Alaska, and Alaskan Stream

The Alaskan Stream is the primary circulation feature of the southern Pacific-Arctic Region. It is an intense, narrow (~50–80 km) and deep (>3,000 m) current, which flows westward from the head of the Gulf of Alaska to the westernmost Aleutian Islands (Stabeno and Reed 1992; Reed and Stabeno 1999). Its highly variable transport (e.g. Onishi 2001) reflects the complex air-sea-topographic interactions in the northern North Pacific and strongly influences the exchanges with the Bering Sea (Maslowski et al. 2008a; Clement Kinney and Maslowski 2012), which occur through the straits and passes of the Aleutian-Komandorskii Island Arc.

The transport estimates of the Alaskan Stream based on observations (Thompson 1972; Favorite 1974; Reed 1984; Stabeno and Reed 1992; Reed and Stabeno 1993, 1997) are generally limited by coarse or intermittent temporal and/or spatial sampling. Such limitations hinder investigations of local dynamics, long-term mean total volume and property fluxes and relationships between climate change and transport variability. The deep baroclinic structure and the westward intensification (between 150°W and 180°W; Reed 1984) of this boundary current flowing along the slope of the Aleutian Trench present further challenges for transport estimates based on spatially limited measurements using geostrophic velocity calculations, where an assumption of no motion at depth (e.g. at 1,000 or 1,500 m compared to the total depth of over 6,000 m) is made. For example, Reed (1984) computed a typical transport in the Alaskan Stream (referred to 1,500 dbar) at 12 Sv ($1 \text{ Sv} = 10^6 \text{ m}^3 \text{ s}^{-1}$) and at 15–20 Sv when a correction for its baroclinic structure below 1,500 dbar is included. Other commonly reported transports (Royer and Emery 1987; Reed 1984; Reed and Stabeno 1999) are all estimated below 25 Sv, including corrections for the deep baroclinic flow. However, accurate assessment of the total volume transport at any cross section in the Alaskan Stream is still daunting, as it requires knowledge of the absolute velocity structure down to the bottom.

The chain of the Aleutian Islands forms the natural southern boundary of the Bering Sea. The numerous passes between islands play a primary role in determining both circulation and distribution of water properties in the Bering Sea (Stabeno et al. 1999). The variability of the inflow/outflow rate through the southern boundary has a twofold impact on Bering Sea oceanic conditions and ecosystem changes. First, inflow through Aleutian passes is an important source of Bering Sea ecosystem nutrients (Stabeno et al. 1999). Second, strong inflow through the Amchitka, Amukta, and other Aleutian passes may enhance instability of the Aleutian North Slope Current (ANSC) and thus affect Bering Sea eddy formation.

Although the eastern passes are shallow, with depths less than 300 m, the long-term velocity observations in several passes indicate strong and persistent northward flow. For example, Stabeno et al. (2005) reported approximately 4 Sv of mean inflow into the Bering Sea through Amukta Pass during a period of 3 years (2003–2005), which is approximately five times larger than geostrophic estimates (Stabeno et al. 1999). Thus, recent estimates indicating higher exchange rates between the

Bering Sea and Pacific Ocean require extended studies of the robustness of these estimates and, possibly, revising our view on the mechanisms controlling Bering Sea circulation.

Modeling the Alaskan Stream and the inter-basin exchanges between the North Pacific and the Bering Sea has been challenging, as well. Ocean general circulation models (OGCMs) have demonstrated a rather limited ability to realistically represent circulation and inter-basin exchanges of water mass and properties between the North Pacific and the Bering Sea/Arctic Ocean. While global models have commonly lacked the needed horizontal and/or vertical resolution (e.g. Goosse et al. 1997; Xie et al. 2000) regional models of this region have often used closed or fixed (prescribed) boundary conditions in the Bering Sea and/or North Pacific (Overland et al. 1994; Hurlburt et al. 1996; Stabeno and Hermann 1996; Okkonen et al. 2001; Hermann et al. 2002; Ladd and Thompson 2002). Additionally, only few of those models have realistically accounted for the net northward transport (0.8 Sv ± 0.2 Sv; Clement Kinney et al. 2014, this volume) through Bering Strait (e.g. Goosse et al. 1997).

The NAME model has been developed to address the above limitations and to allow focused studies of the circulation, relevant dynamics and exchanges between the sub-arctic and arctic basins (Maslowski et al. 2004, 2008a; Clement et al. 2005; Clement Kinney et al. 2014, this volume). The pan-Arctic domain of this model, (Fig. 5.2) configured at horizontal resolution of 1/12° and 45 depth levels allows for realistic flow through the many narrow passages in the Aleutian Islands and the northern Bering Sea.

Figure 5.3 shows the 26-year (1979–2004) mean circulation in the upper 100 m based on NAME model results (Clement Kinney and Maslowski 2012), in which the Alaskan Stream is clearly the strongest feature. The Alaskan Stream is the primary source of warm and relatively fresh water for mass and property fluxes through the Aleutian passes and, therefore, has a significant influence on the Bering Sea (Reed 1990; Reed and Stabeno 1999).

NAME model results (not shown) in the upper 100 m of the Alaskan Stream show that maximum speeds close to 90 cm s^{-1} occur in winter (i.e. January, February, March), with a decrease to around 75 cm s^{-1} in summer and autumn, suggesting up to 14 % speed variability due to the seasonal cycle. According to observations, Reed and Stabeno (1997) report 70–125 cm s^{-1} speeds in the upper 100 m across 173.5°W measured during summer 1995. Reed (1984) obtained similar peak speeds (90–110 cm s^{-1}) in the upper ocean across 170°W during winter 1980 and summer 1981. Reed and Taylor (1965) measured velocities of 80 cm s^{-1} around 175°W in June 1959. The above comparison of modeled and observed velocities in the upper 100 m of the Alaskan Stream suggests the model realistically represents this flow.

The modeled 23-year mean westward transport of Alaskan Stream computed over the total water depth ranges from 44.6 Sv to 55.8 Sv, of which 12–18 Sv is below 1,000 m and 7–12 Sv is below 1,500 m. These transports appear rather high compared to the previously reported estimates based on measurements; however some observational evidence exists in support of higher model results. Warren and
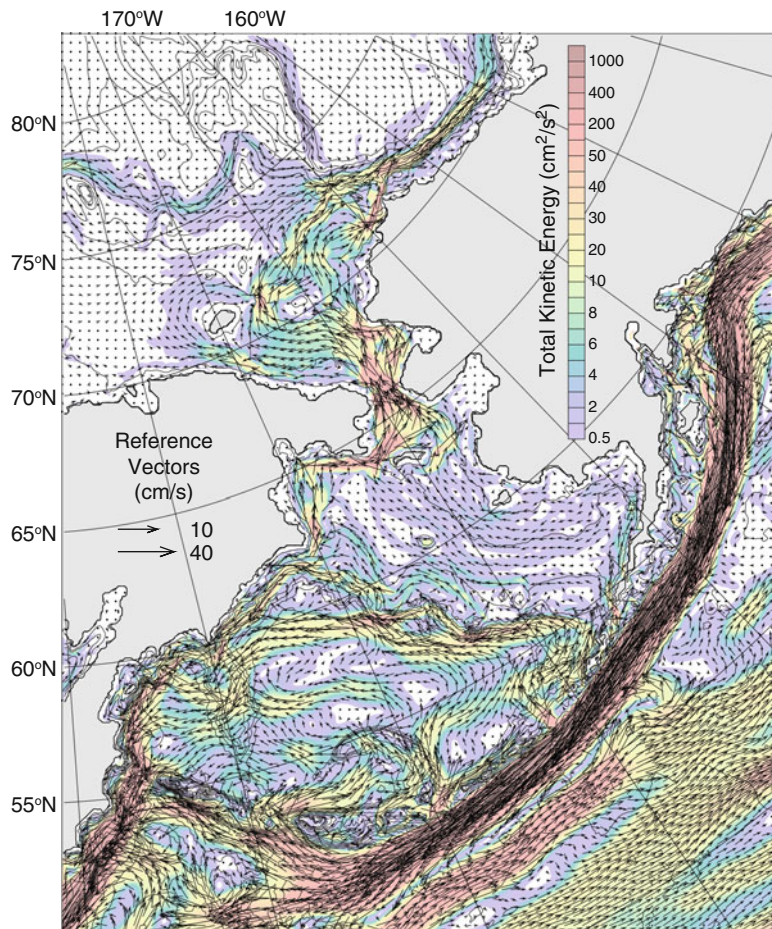
Fig. 5.3 The 26-year mean (1979–2004) upper 100 m modeled circulation (*vectors* shown every 4th grid cell in each direction; cm s⁻¹) and total kinetic energy (*shading*; cm² s⁻²). *Black contour lines* represent bathymetry (m). Please note that the velocity vectors are not scaled in a linear fashion (for figure clarity) and their magnitude can be derived as $|v| = (2 \times TKE)^{1/2}$

Owens (1988) reported 28 Sv based on geostrophic calculation but referred to current meter measurements from a single mooring. Hydrographic measurements by Roden (1995) near 180°W indicate transport of 38 Sv above 6,000 m with 14 Sv below 1,000 dbar and 9 Sv below 1,500 dbar in July 1993. Onishi and Ohtani (1999) computed the Alaskan Stream transport ranging from 21.8 Sv to 41 Sv along 180°W during 1990–1997. Finally, Onishi (2001) estimates the transport referred to 3,000 m ranging from 14.8 Sv to 41.0 Sv along 180°W over 9 years, from 1990 to 1998.

Major disturbances created by southward shifts in the Alaskan Stream and eddies propagating along the Aleutian Island Arc can produce large deviations, which have

been explored in multiple studies (e.g. Musgrave et al. 1992; Stabeno et al. 1999; Crawford et al. 2000). In Crawford et al. (2000), 6 years of TOPEX/Poseidon (T/P) data measured the presence of six anticyclonic eddies in the Alaskan Stream. Of the six eddies, some formed near the Alaskan panhandle, while others began propagating just south of Shelikof Strait with an estimated phase speed of ~2.5 km/day. The sea surface height anomalies and eddy diameter approached 72 cm and averaged 160 km, respectively. Because the Alaskan Stream represents the largest source of transport into the Bering Sea, these long-lived eddies (mean lifespan of 1–3 years; Crawford et al. 2000) may significantly alter both the physical and biological structure of the Bering Sea (Okkonen 1992, 1996).

Recent model results (Maslowski et al. 2008a) provided an in-depth examination of the anticyclonic eddies found in the Alaskan Stream and their effect on the strength and location of the stream, as well as their influence on flow through Amukta and Amchitka Passes. For example, sea surface height anomaly (SSHA) and circulation (Fig. 5.4a) indicate the presence of an anticyclonic eddy south of Kodiak Island during January 1993. By December (Fig. 5.4b), the eddy has moved to a position that is just southeast of Amukta Pass. Figure 5.5 shows modeled monthly mean distributions of velocity as the eddy passes by EAS1 during January 1993 and EAS4 during December. In both cases, the velocity core is shifted southward when the eddy is present. The southward shift is strongest at EAS4 by a distance of more than 140 km. Over the course of the entire model simulation (1979–2003), the number of eddies crossing the EAS4 line was calculated (Maslowski et al. 2008a). Twenty "weak" eddies (0.3 m<SSHA<0.5 m) crossed the line for an average of 0.8 per year and 12 "strong" eddies (SSH>0.5 m) were identified for an average of 0.5 per year.

Using a combination of these model results, additional model results from Maslowski et al. (2008a), and observational results by Reed and Stabeno (1989, 1999) and Crawford et al. (2000), we conclude that the Alaskan Stream remains relatively intact during the periods of southward shifts. It is also believed that the formation and propagation of eddies along the Alaskan Stream is the main cause of these deviations in the westward flow. Any stationary attempt to monitor the flow of the Alaskan Stream (e.g., moored Acoustic Doppler Current Profiler (ADCP)) would benefit from including instrumentation at least 200 km southward of the mean position of the Alaskan Stream, in order to capture these shifts.

Investigation of eddy effects on exchanges between the Gulf of Alaska and the Bering Sea revealed significant increases in net northward fluxes as an eddy moves along a pass within the Aleutian Islands (Maslowski et al. 2008a). Analysis of modeled time series through the two main passes in the eastern and central Aleutian Archipelago, i.e., Amukta Pass and Amchitka Pass, showed that peaks in the monthly mean anomalies of volume and property transport were often associated with the presence of nearby eddies in the Alaskan Stream (e.g. see Fig. 5.9 in Maslowski et al. 2008a).

Another dynamical aspect of the Aleutian throughflow, which should be taken into account, is tidal mixing and rectification. Tidal currents between the Aleutian Islands are generally strong (100–150 cm/s) and produce a total 70 GW energy flux
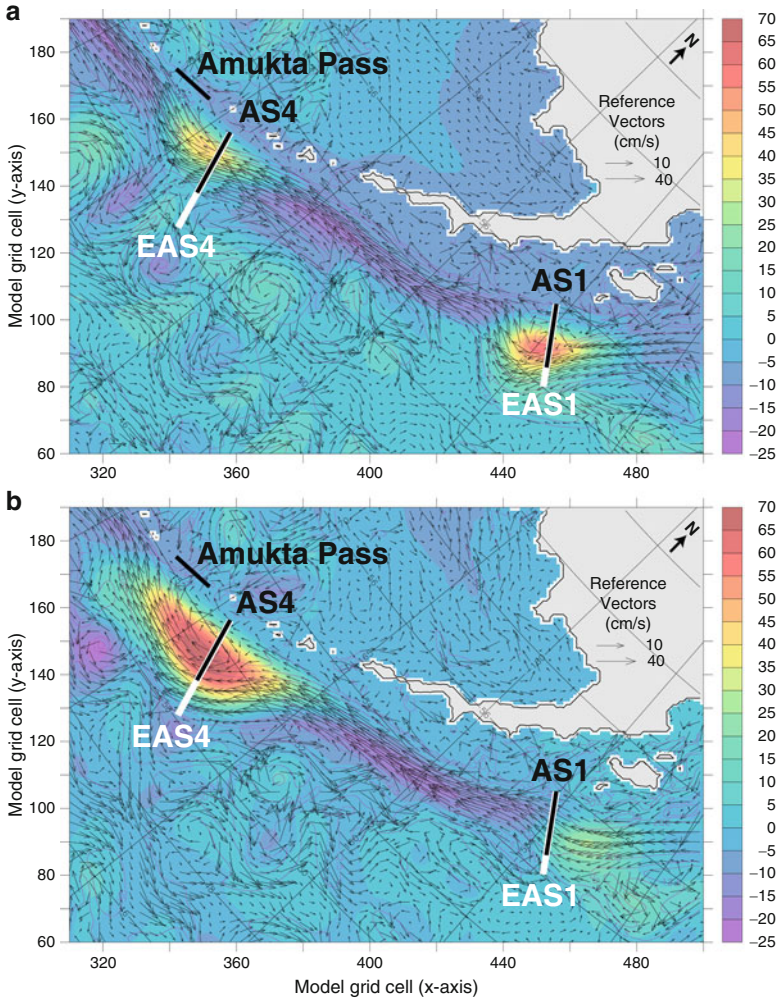
Fig. 5.4 Modeled sea surface height anomaly (m) and 0–477 m circulation during (**a**) Jan. 1993 and (**b**) Dec. 1993. Every 3rd *vector* in each direction shown

into the Bering Sea (Foreman et al. 2006). The most important are the M2 (31 GW), K1 (24.5 GW) and O1 (13 GW) tidal constituents (Foreman et al. 2006). The largest energy conduits into the Bering Sea are via Amukta and Samalga passes (M2) and Amchitka Pass (K1). Modeling studies (e.g. Kowalik 1999) show that tides significantly impact local mixing and generate a northward residual tidal current of 5–15 cm/s between the Aleutian Islands. Recently, Stabeno et al. (2005) hypothesized that tidal rectification may be one of mechanisms responsible for such a high new mean inflow through Amukta Pass.
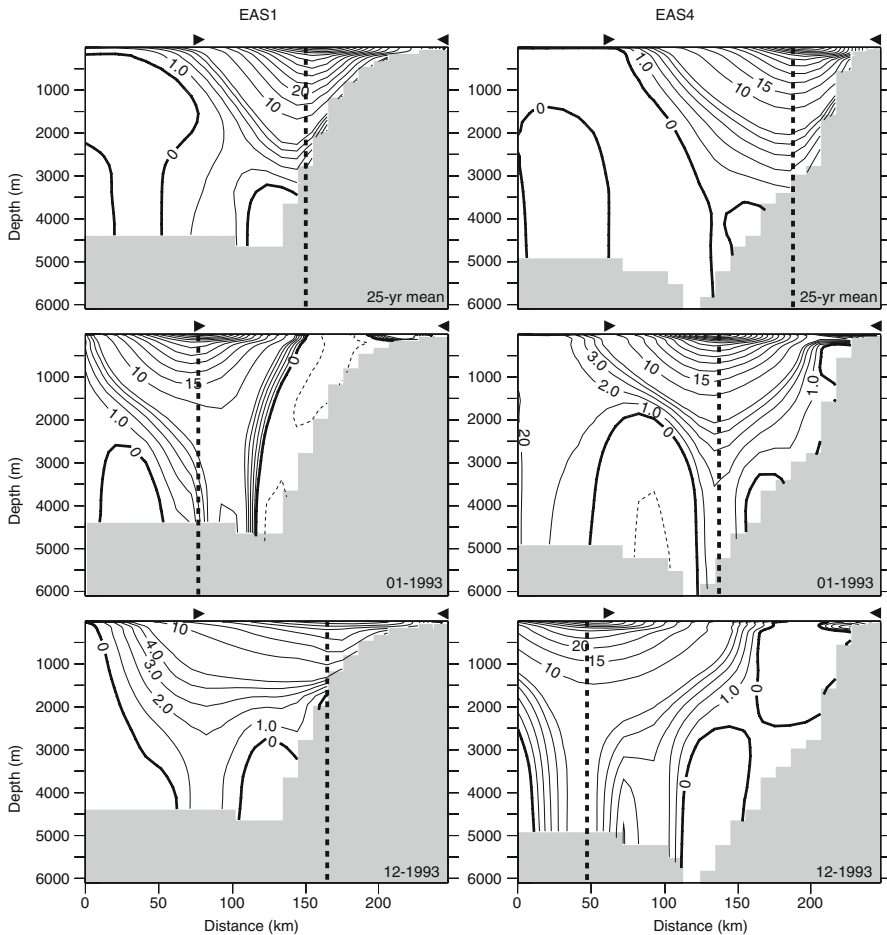
Fig. 5.5 Modeled monthly mean vertical profiles of velocity (both *shading* and *contours*; cm s⁻¹) for cross sections EAS1 (*left*), EAS4 (*right*). Positive velocity is directed westward. Inward-facing *triangles* above each figure indicate the position of the original sections (AS1 on *left*; AS4 on *right*). The *black line* represents the horizontal position of the velocity core

5.3 Western Subarctic Gyre

Focusing on the deep western passes, we know that inflow from the northwestern North Pacific into the Bering Sea occurs primarily through Near Strait, while outflow occurs largely through Kamchatka Pass (Stabeno and Reed 1994). Multi-year continuous observations of the flow through the western Aleutian Island Passes are not available. Available observations include data from satellite-tracked drifters (Stabeno and Reed 1994) and short-term CTD measurements (e.g. Stabeno and Reed 1992; Reed and Stabeno 1993), along with historical datasets (e.g. Arsen'ev 1967; Ohtani 1970; Hughes et al. 1974; Favorite 1974). Observed estimates of the

net volume transport through Near Strait are northward and range from ~5 Sv (Reed and Stabeno 1993) to ~10 Sv (historical measurements by Favorite 1974). The long-term mean model result from NAME (5.06 Sv) compares well with the observations from Reed and Stabeno (1993).

Observed estimates of the net volume transport through Kamchatka Strait are southward and range from ~6 to 15 Sv (Ohtani 1970; Verkhunov and Tkachenko 1992; Stabeno and Reed 1992). The long-term mean model result from NAME (8.9 Sv) is within the observed range, however it is much less than recently published results from Panteleev et al. (2006). Panteleev et al. (2006) fulfilled variational analysis of the summer climatological circulation in the major part of the Bering Sea. They estimated the volume transport through Kamchatka Strait to be 24 Sv, which is significantly larger than most of the traditional dynamical method estimates (Ohtani 1970; Verkhunov and Tkachenko 1992; Stabeno and Reed 1992). On the other hand, the Panteleev et al. (2006) transport estimate agrees well with an estimate by Hughes et al. (1974) of 20 Sv, obtained through dynamical calculations referenced to the surface velocities taken from surface drogued floats.

High-resolution and large scale modeling of the Bering Sea basin and the Western Subarctic Gyre has been limited. Previous modeling work by Overland et al. (1994) realized general circulation features (e.g., complex cyclonic flow in the Bering Sea basin) similar to observations. However, they were not able to simulate the meanders in the Kamchatka Current that were identified by Stabeno and Reed (1994), nor were they able to show enough interannual variability in the flow through Near Strait to account for observations by Stabeno and Reed (1992) or Reed et al. (1993). The prescribed boundary condition for the Alaskan Stream and the climatological atmospheric forcing that was used may have prevented Overland et al. (1994) from simulating realistic variability in the flow through Near Strait. While observations before 1994 (e.g., Reed 1984; Stabeno and Reed 1992) showed little eddy energy of the Alaskan Stream near 166°W (i.e. the lateral boundary of the Overland et al. (1994) model domain), more recent observations (e.g. Crawford et al. 2000) are in stark contrast.

Recent modeling work by Clement Kinney and Maslowski (2012) shows how the numerous eddies and meanders of the Bering Sea and within the Alaskan Stream play a critical role in determining the flow through the western Aleutian passes and straits. For example, modeled time series of volume flux through Near Strait over 26 years showed seven time periods when the transport was near-zero or even reversed (Clement Kinney and Maslowski 2012). These anomalies lasted from 3 months to almost 2 years. Based on satellite-tracked drifters released throughout the region, Stabeno and Reed (1992) noted an anomalous lack of inflow through Near Strait that began in summer 1990 and persisted at least through fall 1991. While the model results did not show a lack of inflow at exactly the same time period as Stabeno and Reed (1992), the processes underlying the anomaly appear to be the same. The modeled flow reversals and maxima were related to the presence of eddies and meanders both north and south of the strait. There did not appear to be a consistent circulation regime responsible for inducing a reversal (see Clement Kinney and Maslowski (2012) for further discussion and figures). Instead, flow

reversals occurred when mesoscale features were in the proper alignment with the axis of the strait. Therefore, it is believed that short-term observations (months to years) may not be representative of the actual mean flow. This indicates a need for continuous monitoring of the flow through Near Strait, as well as other passes and straits in the Western Aleutian Islands to determine both the mean flow and its variability.

5.4 Bering Sea

The general circulation within the Bering Sea basin is typically described as cyclonic in the long-term mean. However, transport within the gyre can vary by more than 50 % (Stabeno et al. 1999). Causes associated with this variation have been identified as either changes in the Alaskan Stream inflow (Overland et al. 1994) and/or variability of the wind-driven transport within the basin (Bond et al. 1994). Mesoscale eddies within the basin have been identified in observations published by Cokelet et al. (1996) and Stabeno and Reed (1994), among others (e.g., Solomon and Ahlnäs 1978; Kinder et al. 1980; Paluszkiewicz and Niebauer 1984). Instabilities along the Bering Slope and Kamchatka Currents and interactions with canyons and embayments at the landward edge of these currents and inflows through the Aleutian Island Passes may be responsible for eddy generation (Cokelet et al. 1996). Stabeno and Reed (1994) observed several eddies and meanders within the Kamchatka Current and the eastern Bering Sea by utilizing satellite-tracked drifters. Several anticyclonic eddies were observed in the western side of the basin and resulted from the interaction of the Kamchatka Current with topographic features. Stabeno and Reed (1994) suspect that these features are semi-permanent, since they appeared in drifter trajectories for more than 1 year. Stabeno and Reed (1994) observed a large anticyclonic eddy west of Bowers Ridge that had a diameter of approximately 200 km and velocities of 30–40 cm/s, which is similar in size and velocity to those from the NAME model.

Animations of monthly mean NAME model results over the 26-year simulation show frequent and complex eddy activity throughout the Bering Sea basin. For instance, at least 14 mesoscale eddies are present in June 1987 (Clement and Maslowski 2008), as shown in Fig. 5.6. Half of these are anticyclonic and the other half are cyclonic. Diameters of these eddies are 120 km and greater and velocities are up to 40 cm/s. Lifetimes of these eddies are typically a few months. The 9-km horizontal resolution of the model makes it possible to resolve eddies with diameters as small as ~37 km, however, the smallest eddies are likely not resolved, recalling that the Bering Sea has a Rossby radius of deformation of ~12–20 km according to Chelton et al. (1998).

During the 26-year model simulation, meanders and eddies are continuously present throughout the deep Bering Sea basin. This is consistent with results from Cokelet and Stabeno (1997), which show that the background flow in the interior of the Bering Sea is dwarfed by the energetic eddies which populate the region.
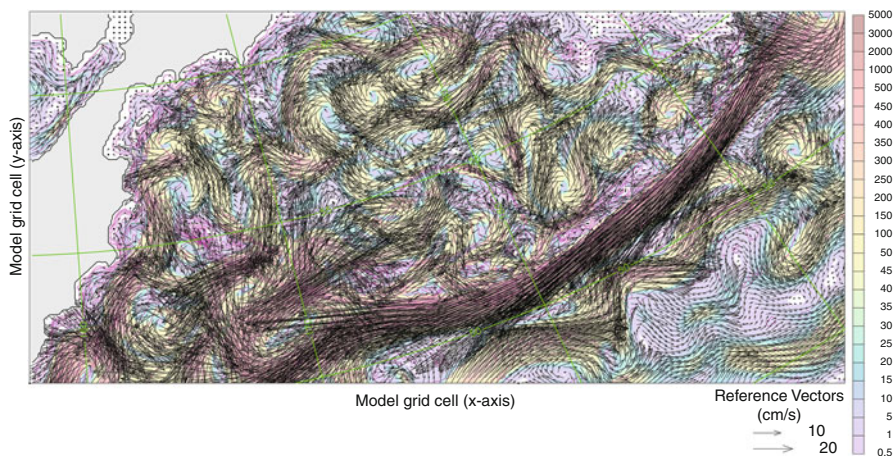
Fig. 5.6 The June 1987 upper 100 m mean modeled circulation (*vectors*) and total kinetic energy (*shading*; cm^2 s^{-2}). *Magenta contour lines* represent bathymetry (m). Every 3rd *vector* in each direction shown

Our results indicate that these eddies are important in redistributing temperature and salinity (Clement Kinney and Maslowski 2012), which may have an effect on biological species in the region by altering environmental conditions.

Numerical model results (Clement Kinney and Maslowski 2012) also show very frequent and complex eddy activity present along the Bering Sea Slope. In fact, the Bering Slope Current (BSC) appears to be more a system of eddies rather than a continuous feature (Okkonen 1993; Clement Kinney et al. 2009). The energetic anticyclonic eddy activity of the BSC is a well-known characteristic of Bering Sea circulation. Analysis of the mooring velocity measurements along the eastern Bergin Sea continental slope between Pribilof and Zhemchug canyons (Schumacher and Reed 1992; Cokelet and Stabeno 1997) showed that mesoscale currents have amplitude >80 cm/s, i.e. 10–15 times higher than the long-term mean BSC velocity. The BSC eddies penetrate to a depth of at least 500 m and transport nutrients from deep regions onto the eastern Bering Sea shelf (Stabeno et al. 1999). Eddy-induced cross-shelf mixing is not well studied, but high-intensity mesoscale variability in the region indicates the importance of this mechanism. Recent climatological studies reveal the linkage between long-term variability of the large-scale dynamic and oceanic eddy activity (Hogg et al. 2005). Currently the mechanisms of this linkage are not clear.

The eddy activity along the Bering Sea slope seems to have an important effect on shelf-basin exchange, especially in canyons such as Zhemchug Canyon (Clement Kinney et al. 2009). A cyclonic eddy located just south of the canyon was shown to greatly increase the on-shelf salt flux during a 3-month period via upwelling of relatively salty water and on-shelf flow. Upwelling of salty and nutrient-rich deep Bering Sea water due to eddies and shelf-basin exchange, in general, could enhance biological production in this region (Clement Kinney et al. 2009). Overall circulation over the

Bering Sea shelf is mainly wind-driven and geostrophic year around, with reversals of both across and along shelf flow and local accelerations due to increased wind stress and bottom friction in response to changing winds between northwesterly and southwesterly (Danielson et al. 2012a, b).

Modeled eddy kinetic energy (EKE) fields show that the northern Bering Sea maintains year-round high energy and mixing, especially in Bering and Anadyr straits (see Figs. 5.16–5.19 of Clement et al. 2005). Notably, these regions of high EKE are found just upstream of highly productive areas in the Bering Sea (e.g., the Chirikov Basin and the region just north of Bering Strait) that have been identified in previous studies such as Grebmeier et al. (1988), Springer and McRoy (1993), and Grebmeier and Dunton (2000). This suggests that high-nutrient Anadyr Water is mixed into the euphotic zone as it flows generally northward and, upon encountering a region of lower EKE, can support water column primary production and the settling of organic matter to the benthos.

5.5 Chukchi Sea

The Arctic receives water from the Pacific through the Bering Strait. The Chukchi Sea connects the Bering Sea to the Arctic Ocean and is, therefore, the Pacific gateway to the Arctic. Three primary water masses enter the Chukchi Sea via Bering Strait, including Alaskan Coastal Water, Bering Shelf Water, and Anadyr Water (Coachman et al. 1975). Alaskan Coastal Water, as its name implies, is found near the coast of Alaska and tends to be the warmest and freshest of the three. Anadyr Water is found in the west, nearer to Siberia and is usually colder and more saline than the others. Bering Shelf water lies in the middle and has more moderate temperature and salinity properties. Analysis of a year long time series of mooring data in 1990–1991 by Woodgate et al. (2005) indicates a fourth branch of water inflow through Bering Strait which exits northwestward through Long Strait. Its content of water originating from the Pacific is less than that contributed by the other three branches, as it is modified by the seasonally occurring Siberian Coastal Current (Weingartner et al. 1999). A number of important bathymetric features, such as Herald Shoal, Hanna Shoal, Barrow Canyon, Herald Canyon, the Chukchi Rise, and the Chukchi Cap influence the circulation on this shallow (mostly <60 m deep) and wide continental shelf.

Previous numerical modeling efforts for the Chukchi and Beaufort seas include Overland and Roach (1987), Winsor and Chapman (2004), and Walsh et al. (2004), with the latter based on results from the same model discussed in this article. In addition, all of the models participating in the Arctic Ocean Model Intercomparison Project (AOMIP; e.g. Proshutinsky et al. 2007; Holloway et al. 2007) as well as a recent study by Watanabe (2011) include the Chukchi Sea. However, many of those models prescribe climatological lateral boundary conditions at or near Bering Strait. As for global climate models, their spatial resolution in ocean models is commonly too coarse to realistically represent exchanges through Bering Strait, and they have to be parameterized (e.g. Goosse et al. 1997). An improvement of the NAME

model is the ability to simulate the net northward transport and variability of water mass and properties through Bering Strait (Clement et al. 2005; McClean et al. 2001). Model results from the simulation discussed here have been compared with observations of volume transport, temperature and salinity in Bering Strait. For example, the modeled 1979–2004 mean volume transport of 0.65 Sv compares well with the observed mean of 0.83 Sv estimated for 1990–1994 (Clement et al. 2005; Roach et al. 1995). Please see Clement Kinney et al. (2014, this volume) for a comprehensive discussion of the flow through Bering Strait.

The 26-year (1979–2004) mean circulation from the NAME model in the upper 100 m is shown in Fig. 5.3. Generally northward velocities, as high as 50 cm/s, are found in Bering Strait with three main branches and two coastal flows forming north of the strait. Model results are in agreement with observations at 12 locations within the Chukchi Sea made by Woodgate et al. (2005) that show four northward outflows on the Chukchi Shelf. The main western branch (Herald Valley flow) is found between the 50-m isobaths and flows between Herald Shoal and Wrangel Island. The main eastern branch is directed primarily northward to the east of Herald Shoal and west of the 25-m isobath. This is the "Central Channel" flow identified by Weingartner et al. (2005) based on moored and shipboard data collected in the early 1990s. An offshoot of the western branch flows through Long Strait (between Wrangel Island and Siberia), most of which encircles the island in an anticyclonic fashion and eventually joins the Central Channel flow, however a small portion of the current continues along Siberia to the northwest near the coast. The seasonal, eastward-flowing Siberian Coastal Current (Weingartner et al. 1999) is not clearly showing in the 26-year mean circulation; however, velocity vectors nearest the coast are oriented eastward and snapshots of the ocean circulation (not shown) in early summer (i.e. June–July) have an evident narrow eastward flow. The other seasonal coastal current, modeled with relatively higher skill, is the Alaskan Coastal Current (ACC), which is fresh, warm (with measured temperatures up to 11 °C in August 2007) and narrow (10–40 km; Okkonen et al. 2009; Spall et al. 2008). Still, a more realistic representation of winds and local fresh water discharge from the Siberian and Alaskan coasts as well as higher spatial resolution would further improve model skill in simulating both of these coastal currents (Maslowski and Walczowski 2002; Newton et al. 2008). It is important to note, that observations made by Paquette and Bourke (1974) and Ahlnäs and Garrison (1984) show that the ACC is enhanced by solar-heated waters in Kotzebue and Norton sounds and it impacts the local ice edge position downstream.

Measurements of the oceanic impact on the marginal ice zone and ice edge position in the Chukchi Sea are limited and insufficient to quantify those effects. To address this, a series of cross-sections were established in the NAME model to obtain volume and relative heat flux values from the 26-year long integration (Fig. 5.7). The blue ACC sections were intended to capture the coastal flow, while the CL sections capture the north-south flow across the width of the Chukchi shelf. The CP sections, along with CL4, form a closed polygon surrounding the Chukchi Plateau. Table 5.1 shows the mean volume transport, heat flux and temperature across each
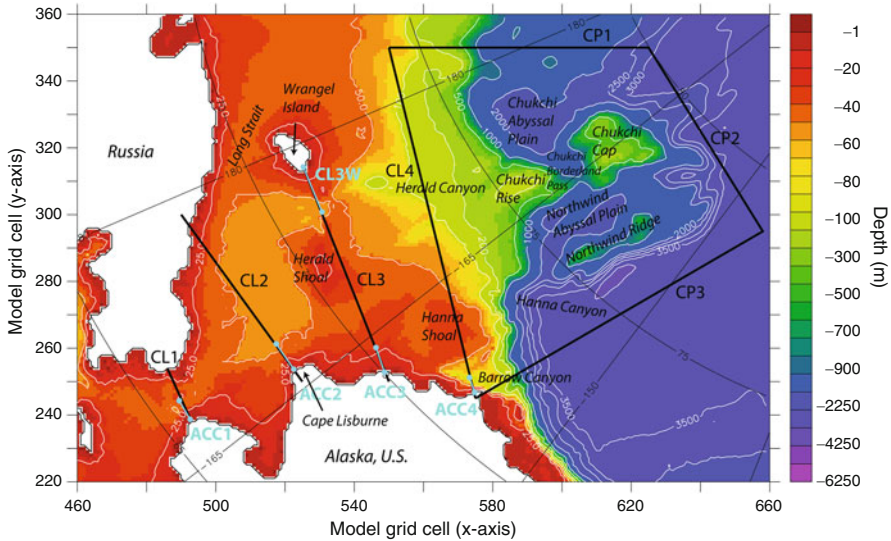
Fig. 5.7 Bathymetry (*shading*; in meters) with the locations of a series of cross-sections (*black* and *blue lines*). Labels corresponding to the cross-sections are either shown in *black* for longer sections or *green* for shorter sections. Place names are shown in *italics*

section. The main purpose of this is to determine relative contributions of heat flux across a given section or depth range relative to the total heat divergence/convergence from/into a specified region or basin and its relative change in time. In particular, the heat fluxes calculated here through a single section are not meant to estimate the change of heat in a closed volume as proposed by Schauer et al. (2008).

The coastal flow through ACC1 and ACC2 makes up almost half of the volume transport through the respective CL sections. More than half of the heat flux through CL1 and CL2 is found in the coastal sections (55 % and 71 %, respectively). The relative increase of heat flux between ACC1 and ACC2 supports the finding of Ahlnäs and Garrison (1984) that the solar-heated waters in the Kotzebue Sound and along the coast are some of the main sources of heat in the Alaskan Coastal Current. However, as one moves farther north, little of the heat or volume flux across CL3 is found in the shorter coastal section ACC3. Instead, the majority of the flow is bathymetrically steered away from the coast and to the west of Herald Shoal (Fig. 5.3). Some mixing and convergence of the Herald Valley flow and the Central Channel flow occurs north of Herald Shoal, where the flow becomes bathymetrically steered eastward as observed by Weingartner et al. (2005). Upon reaching Barrow Canyon, much of the heat (~63 % of the CL4 value) is again found near the coast, within section ACC4 (Fig. 5.8). It is also worth noting that both in the modeled coastal flow as well as across the entire CL4 two to three times more heat is transported below 10 m depth relative to the upper 10 m. We argue that over the Chukchi shelf, heat associated with summer Pacific water is partially lost to sea ice melt and to the

Table 5.1 Twenty-six year mean (1979–2004) and standard deviation (*in parenthesis*) for volume transport, heat flux and mean temperature across selected sections

Section	Volume transport (Sv)	Heat flux (TW)	Mean temperature (°C)
ACC1	0.302	2.315	−0.098
	(0.099)	(3.440)	(2.063)
ACC2	0.285	2.344	−0.450
	(0.151)	(3.735)	(1.688)
ACC3	0.014	0.170	−0.653
	(0.032)	(0.464)	(1.519)
ACC4	0.300	0.736	−1.273
	(0.172)	(1.192)	(0.400)
CL1	0.654	4.172	−0.364
	(0.228)	(5.695)	(1.656)
CL2	0.643	3.288	−0.983
	(0.225)	(4.793)	(0.823)
CL3	0.520	1.416	−1.138
	(0.221)	(1.906)	(0.515)
CL3W	0.196	0.305	−1.345
	(0.067)	(0.255)	(0.226)
CL4	0.678	1.167	−1.092
	(0.216)	(1.271)	(0.101)
CP1	0.526	2.509	−0.902
	(0.177)	(0.759)	(0.058)
CP2	−0.206	−0.447	−1.059
	(0.095)	(0.229)	(0.038)
CP3	−0.927	−2.719	−1.052
	(0.309)	(1.674)	(0.087)

Positive direction is north for all sections except CP1 (East), CP2 (South) and CP3 (West). Salinity-dependent freezing temperature was used as a reference temperature for heat flux calculations. Section locations are shown in Fig. 5.7

atmosphere, while it is gained as a result of the ice-albedo effect, as sea ice retreats, allowing increased absorption of solar insulation (as shown in Fig. 5.8). These processes, combined with the complex flow pattern between CL1 and CL4, provide at least a partial explanation for the relatively low correlation of interannual variability between the heat fluxes through Bering Strait and those entering the Beaufort Sea between Barrow and Barrow Canyon (Shimada et al. 2006). Correlation coefficients for modeled monthly mean heat flux anomalies (after removing the mean annual cycle) between ACC1/CL1 and ACC4/CL4 are 0.24/0.38 (Tables 5.2 and 5.3). The fact that the highest correlations for all sections are at no lag implies that atmospheric forcing, including winds, radiative and sensible heat fluxes, is the dominant factor moving and affecting water mass properties and their variability across the Chukchi Sea. These model results also suggest that the oceanic heat flux from Bering Strait has a direct impact on sea ice melt and advancement of the ice edge northward over the Chukchi shelf, but not on the oceanic heat flux farther downstream over the outer shelf, slope, and into the Beaufort Sea.
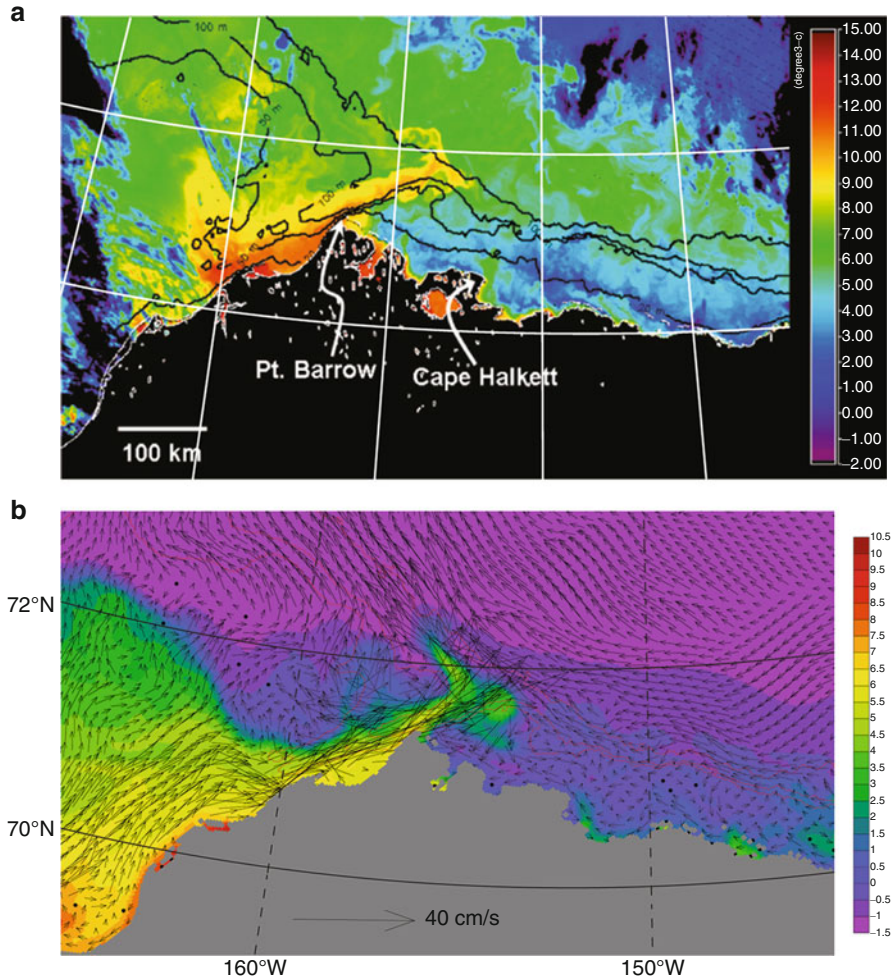
Fig. 5.8 (**a**) Sea surface temperatures (°C) from MODIS for 10 August 2007, 2335UT (Adapted from Okkonen et al. 2009); (**b**) temperature (*shading*; °C) and velocity (*vectors*; cm s^{-1}) at the surface layer (0–5 m) from the NAME model configured at 1/48° (or ~2.3 km) horizontal resolution on 15 August, 1988. The depth contours of 50, 100 and 1,000 m are shown in both panels. Every 10th vector in each direction shown in (**b**)

5.6 Beaufort Sea

Continuing downstream from the Chukchi Shelf, we find a model mean of 0.3 Sv flows northeastward through Barrow Canyon with monthly mean velocities up to 25 cm s^{-1} (Fig. 5.3, Table 5.1). Annually, the warmest waters exiting Barrow Canyon into the Beaufort Sea are typically observed in August–October (Spall et al. 2008; S. Okkonen unpublished data; K. Shimada personal communication). Similarly as

Table 5.2 Correlation matrix for selected ACC sections

Section	ACC1 Absolute	Anomaly	ACC2 Absolute	Anomaly	ACC3 Absolute	Anomaly
ACC2	0.69	0.79	*	*	*	*
	0.94	0.90				
ACC3	0.57	0.42	0.55	0.44	*	*
	0.76	0.58	0.75	0.65		
ACC4	0.73	0.61	0.56	0.43	0.83	0.73
	0.59	0.24	0.62	0.33	0.76	0.67

Correlations are provided for the monthly mean values (absolute) and the anomalies (after removing the annual cycle). The *upper number* in each cell is the correlation coefficient for volume transport and the *lower number* represents the correlation coefficient for heat flux. The lag time of 0 months produces the highest correlation in all instances

Table 5.3 Correlation matrix for selected sections

Section	CL1 Absolute	Anomaly	CL2 Absolute	Anomaly	CL3 Absolute	Anomaly	CL3W Absolute	Anomaly
CL2	0.99	0.99	*	*	*	*	*	*
	0.94	0.93						
CL3	0.94	0.90	0.94	0.90	*	*	*	*
	0.75	0.75	0.85	0.83				
CL3W	0.73	0.64	0.73	0.64	0.76	0.68	*	*
	0.26	0.43	0.33	0.45	0.54	0.58		
CL4	0.93	0.89	0.93	0.89	0.95	0.93	0.76	0.68
	0.70	0.38	0.68	0.45	0.72	0.64	0.41	0.58

Correlations are provided for the monthly mean values (absolute) and the anomalies (after removing the annual cycle). The *upper number* in each cell is the correlation coefficient for volume transport and the *lower number* represents the correlation coefficient for heat flux. The lag time of 0 months produces the highest correlation in all instances

in the Chukchi Sea, hydrographic observations off Barrow describe the cold and fresh surface layer due to ice melt with relatively warmer water below (Fig. 5.9). Pacific summer water (PSW) is typically defined by a temperature maximum within salinity range $31 < S < 33$ (Steele et al. 2004; Sumata and Shimada 2007). As this water leaves the Chukchi shelf it converges with water of the boundary current (Rudels et al. 1994; Woodgate et al. 2001; Nikolopoulos et al. 2009) along the shelf-break and flows along the northern coast of Alaska to the east. A portion of PSW enters the basin and moves northward towards and along the eastern flank of the Northwind Ridge (Shimada et al. 2006; Sumata and Shimada 2007) with mean velocities up to 1.6 cm s^{-1} and the highest subsurface temperatures observed in January (Shimada et al. 2001). The importance of this outflow is clearly demon-strated in Fig. 5.8, where observed surface temperatures within the ACC in August 2007 are almost twice as high as the temperatures of ambient water throughout the northern Chukchi and southern Beaufort seas. While ocean surface temperatures increase due to the ice-albedo effect, in absence of organized currents such as the
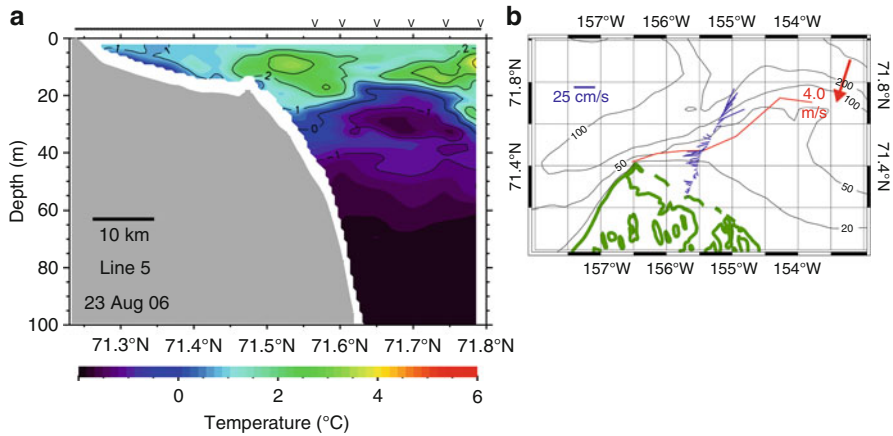
Fig. 5.9 (**a**) Section of observed temperature (°C) along the line from Eielson Lagoon toward the end of Barrow Canyon in the Beaufort Sea on 23 August 2006; (**b**) towed ADCP-measured surface (3–20 m averaged) current vectors along the same section in the Beaufort Sea as in (**a**) (Adapted from Okkonen et al. 2009). The 'v's identify locations of individual CTD casts. The *solid line* identifies the latitudinal extent of sampling by a CTD mounted on a towed undulating vehicle

ACC, their impact on sea ice remains relatively limited. This northward-spreading water, along with associated eddies, is important for introducing relatively warm water into the Canada Basin, which is further discussed below.

The mean ocean circulation in this region is controlled by synoptic, seasonal and interannual atmospheric variability. Okkonen et al. (2009) identified four generalized wind regimes and associated circulation states based on August–September 2005–2007 observations near Barrow, Alaska, combined with numerical simulations for large-scale and long-term context. They found that when winds are weak or from the southwest, PSW intrudes onto the shallow western Beaufort shelf with the majority of PSW flowing eastward along the Beaufort shelf break, while easterly winds favor a more diffuse flow of PSW to the north and northwest, possibly via mesoscale eddies. Moreover, large seasonal variability exists in both water properties exported from the Chukchi Sea and their distribution in the Beaufort Sea (e.g. Münchow and Carmack 1997; Weingartner et al. 1998; Pickart et al. 2005; Spall 2007). In particular, winter-transformed Pacific water is critical to the maintenance of the cold halocline in the Arctic Ocean (Aagaard et al. 1981; Cavalieri and Martin 1994; Chapman and Gawarkiewicz 1995), however its formation and circulation in the western Arctic are not discussed in detail here, as this water mass does not have a direct impact on sea ice.

Recent studies (Spall et al. 2008) estimate that at any time there could be 100–200 eddies in the western Arctic and they could distribute waters originating from the Chukchi shelf (Pickart et al. 2005). Zhang et al. (1999), using an 18-km ice-ocean model, demonstrated that mesoscale ocean eddies play a role in reducing ice concentration and thickness in the western Arctic, in particular along the Chukchi shelf break and the Northwind Ridge. Coincidently, Maslowski et al. (2000) using
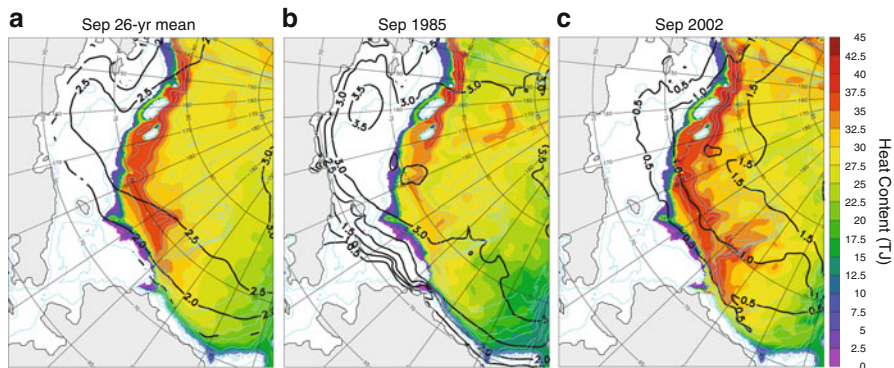
Fig. 5.10 Modeled September monthly mean heat content (TJ; *shading*) at depth 50–120 m and ice thickness contours (m; *black*) for (**a**) 26-year mean, (**b**) 1985 and (**c**) 2002. Bathymetry (m) contours are shown in *blue*

the same model simulated a cyclonic shift in the distribution of Pacific-origin water that accumulated in excess over the Northwind Ridge and along the Chukchi/Beaufort slope between the positive and negative phases of the Arctic Oscillation (AO).

Although the NAME model with horizontal resolution of 9-km does not resolve the smallest eddies (with radius of 10-km or less), larger eddies (with radius of 25 km or more) are commonly simulated in the Canada Basin (Fig. 5.10; Maslowski et al. 2008b). In addition, this limitation is currently being further investigated using the NAME model configured at horizontal resolution of 1/48°. Results from the ongoing model spinup show that at this resolution the model simulates the boundary current around 70 km wide, the ACC between 20 and 30 km wide as well as eddies with radius less than 10 km (Fig. 5.8b). The modeled eddies have variable sizes and origins, however there is a tendency for anticyclonic warm core eddy generation at the mouth of Barrow Canyon and along the Northwind Ridge. The mean core temperature of these eddies at depths of 60–120 m is as much as 1.65 °C above the freezing temperature. The frequency of their occurrence and properties including rotational speeds and temperature are commonly underestimated due to both the spatial resolution limitations and the realism of prescribed atmospheric forcing. However, we believe that the model realistically approximates physical processes that provide sources of heat to the Canada Basin. Based on Figs. 5.8, 5.9 and 5.10, we argue that ocean currents, including mesoscale eddies and topographically driven flow, are important means for distributing warm water and basal melting of the ice pack in the western Arctic.

It is important to note that heat can also be accumulated below the surface mixed layer locally in the Canada Basin, as the sea ice cover continues to retreat farther north and allows increased radiative fluxes into the upper ocean. This is due to the fact that the sunlight can penetrate below the ocean surface. The depth to which the upper ocean can receive heat from the sun depends on the rate at which sunlight is attenuated. It also depends on the wavelength with short wavelengths able to penetrate deeper in the water. Ultimately, in the absence of sea ice, sunlight can often

penetrate below the depth of the surface meltwater layer, typically of order 10–15 m thick. Data from summer CTD surveys by icebreaker and from Ice Tethered Profilers (ITP) during 2005–2010 suggest that a near surface temperature maximum (NSTM) can develop in June–July, when solar radiation is at maximum, as a result of trapping heat below the surface mixed layer due to the onset of summer halocline with ice melt (Jackson et al. 2011, 2012). Given the generally insufficient model spatial resolution and limited observations of eddy generation and transport, estimates of eddy-driven shelf-basin heat transport and its redistribution in the western Arctic Ocean are not available at present. We argue that a quantification of this heat source and understanding of its impact on sea ice are needed to explain the regional differences in arctic sea ice decline and to constrain global climate model simulations and predicted scenarios of future arctic climate change.

5.7 Heat/Freshwater Content and Sea Ice

The outflow of warm summer water from the Chukchi and East Siberian shelves plus local absorption of solar radiation, ocean circulation and mixing contribute to the upper ocean (defined above 120 m) heat content in the western Arctic (west of the Lomonosov Ridge). The heat accumulation in the region has significantly increased since the late 1990s according to observations (Shimada et al. 2001, 2006; Jackson et al. 2012) and the NAME model. In Fig. 5.10 we show modeled heat content at depth 50–120 m and ice thickness in the western Arctic for September 26-year mean, September 1985 (for a typical past cold summer) and September 2002 (a warm summer) to determine potential coherence between these two parameters. The 26-year mean modeled ice thickness in September is about 2.0 m between 72 and 73°N in the Beaufort and Chukchi seas and it extends as far south as 71°N in the East Siberian Sea. The ice becomes thicker than 2.5 m roughly 200–300 km farther north. The 26-year mean oceanic heat content is largest (>30 Tera-Joules (TJ)) over the continental slope and it appears to be associated with the cyclonic boundary current flow carrying summer waters from the Chukchi, East Siberian and Laptev shelves and possibly some contribution of Atlantic water (Polyakov et al. 2010). This heat content maximum spreads eastward towards the Barrow Canyon and northward over the Chukchi Rise and Northwind Ridge and, as shown below, roughly coincides with regions in which the changes in mean ice thickness are greatest.

In September of 1985 (i.e. during a cold summer; Fig. 5.10b) ice was present farther south and thicker in the region (0.5–1.0 m thicker or on average 2.5–3.0 m and up to 3.5 m in the East Siberian Sea) compared to the modeled ice thickness climatology. The modeled heat content during that time was respectively lower, with the maximum over the Chukchi Rise and Northwind Ridge around 5 TJ lower compared to modeled September climatological heat content. Note that even during this cold summer, eddy-like mesoscale features with higher heat content can be seen over the Chukchi Cap and close to the Alpha and Northwind (not labeled in any figure) ridges.
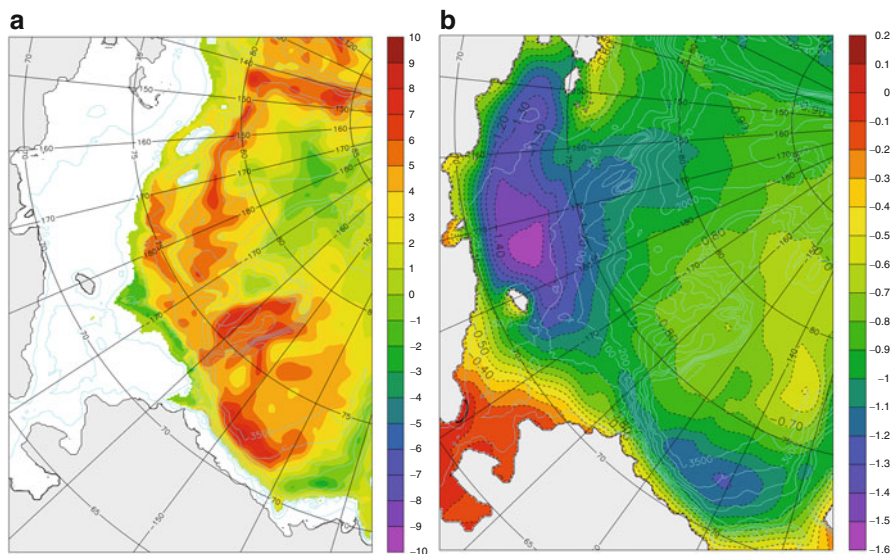
Fig. 5.11 Modeled changes in (**a**) heat content (TJ) at depth 33–120 m and (**b**) sea ice thickness (m) between the mean of 1979–1998 and the mean of 1999–2004

In contrast, 2002 was a relatively warm year with little and thinner sea ice found in the region (Fig. 5.10c). In particular, the thick sea ice over the East Siberian Sea, evident in 1985, has almost disappeared in 2002 leaving open water west of Wrangel Island. Ice thickness between 72 and 73°N is 0.5–1.0 m and only 1.5 m up to 80°N. Coincidently, upper ocean heat content is >30TJ all over that region with a maximum exceeding 40TJ over the continental slope. Recent observations (K. Shimada, personal communication; Jackson et al. 2012) suggest continuing increase of heat content in the western Arctic Ocean, at least through 2010.

A comparison of changes in sea ice thickness and heat content above 120 m between the 20-year mean (1979–1998) and the recent past 5-year mean (1999–2004) is shown in Fig. 5.11. The most striking features in the comparisons of changes in sea ice thickness and heat content above 120 m between the 20-year mean (1979–1998) and the recent past 5-year mean (1999–2004) (Fig. 5.11) are the maximum differences in both sea ice thickness and heat content in the southern Beaufort Sea (140°W–155°W and 71°N–74°N). The reduction in ice thickness of over 1.3 m is co-located with the heat anomaly >15 TJ. In addition, high eddy kinetic energy is simulated in this area both in the 9-km (Maslowski et al. 2008b) and in the 2.3-km (not shown) NAME models. Coincidently, this is also the area where multi-year sea ice has been disappearing and ice cover retreating in summer, despite the increased import of thick and old ice from the region to the north of the Canadian Arctic Archipelago (Stroeve et al. 2011). Finally as discussed below, the maximum freshwater content is co-located in the same region of the Beaufort Sea.
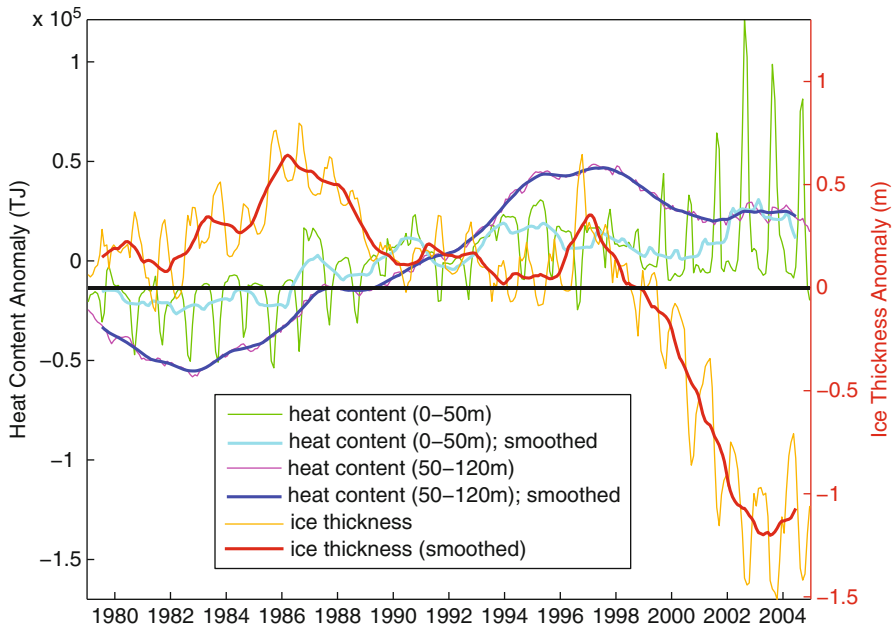
Fig. 5.12 Modeled monthly mean time series of heat content anomaly (TJ) at 0–50 m and 50–120 m and mean ice thickness anomaly (m) in the Western Arctic Ocean (region between 145°E and 135°W and between 70°N and 78°N). Anomaly values equal the annual cycle value subtracted from the monthly mean

The largest sea ice reduction occurring over the East Siberian shelf is associated with a relatively smaller increase in heat content, in part because of its shallow location where long-term heat accumulation is significantly restricted. However, even there increased heat content in the range of 5–10 TJ above the 1979–1998 mean is present on the outer shelf northward of the 100-m isobath and positive heat content anomaly exists southward to the 25-m isobath.

Based on the above results we argue that ocean currents, including mesoscale eddies and topographically driven flow, are important agents for distributing warm water and melting of the overlying ice pack. Next, we analyze time series of heat content in the upper 50 m and at 50–120 m and quantify its negative correlation with sea ice thickness in the Western Arctic Ocean (Fig. 5.12 and Table 5.4). Two depth ranges are defined for these analyses representing the upper ocean (0–50 m) including the surface mixed layer and the pycnocline below and the upper halocline layer (50–120 m). In addition, the surface layer (0–10 m) is considered separately (Table 5.4) as it is most affected by sea ice melt and solar radiation. All correlations between heat content and sea ice thickness shown in Table 5.4 are significant at the 95 % confidence level. For the purpose of this calculation, the Western Arctic Ocean is defined as a region between 70 and 78°N and 145°E–135°W. The region includes the Beaufort, northern Chukchi, and East Siberian seas and accounts for

Table 5.4 Lagged
correlation coefficients of
heat content anomalies in the
top 120 m of ocean with the
mean ice thickness anomalies
in the western Arctic Ocean

Depth range(m)	Monthly Mean (lag)	Summer (JAS) Mean (lag)
0–10	−0.65 (1)	−0.94 (0)
0–50	−0.56 (1)	−0.91 (0)
0–120	−0.69 (50)	−0.87 (37)
50–120	−0.74 (50)	−0.95 (42)

Anomaly values equal the annual cycle value
subtracted from the monthly mean. Positive value
(in months) of lag is for heat content anomalies
leading ice thickness anomalies. Summer months
are July, August, and September (JAS). All correlations
shown in this table are significant at the 95 % confi-
dence level

the majority of observed sea ice reduction in the western Arctic over the past decade.
The heat content time series (Fig. 5.12) indicate that the heat contents were anoma-
lously low prior to ~1990 but increased since the mid-1980s, which was followed
by the loss of excess ice thickness (> 0.5 m) down to more average values through
mid-1990s. Heat contents below 10 m (not shown) increased to above normal since
the early 1990s and have remained elevated with strong summertime peaks in recent
years. It is important to note that especially heat content below 50 m depth has
remained anomalously high, including during winter, since the mid-1990s. In contrast,
waters in the upper 50 m have been releasing all the excess heat every fall/winter.
This implies that the upper halocline layer (roughly 50–120 m) in the western Arctic
has been accumulating heat in winter and making it potentially available for melting
ice from below during the following spring and summer.

Ice thickness shows an overall decreasing trend during the period 1979–2004;
from over 0.5 m above the mean in the second half of the 1980s and in 1996, with a
steady decline below the mean since 1998. Ice thickness anomalies over that region
reached −1 m in winter and −1.5 m in summer during the recent years. It is possible
that a portion of those ice thickness anomalies can be explained by mechanical
redistribution (Holloway and Sou 2002). However, the presence of a heat source
below the ocean's surface (Shimada et al. 2001) must play a role as well. Recently,
Perovich et al. (2008) used autonomous buoys for monitoring thermodynamic mass
balance of the ice and estimated that on average bottom ablation in the Beaufort
Sea ranged from 0.6 to 1.2 m, and in one case reached ~2 m. They concluded that
the positive ice-albedo feedback accelerated the melt of sea ice during the summer
of 2007; however they left an open question as to what triggered the increase of
open water area at the melt onset.

As already mentioned, there is a strong (at the 95 % confidence level) negative
correlation (at positive lag, i.e. heat content anomalies lead ice thickness anomalies)
between upper ocean heat content and ice thickness anomalies (Table 5.4). The cor-
relation coefficients are smaller for all monthly means than for summer months
only. However, correlations of all monthly means might be hard to interpret due to
the fact that heat content anomalies at 0–50 m are reset to zero every winter while

ice thickness anomalies are not reset to any values. For this reason we argue that correlation of summer (July–September) anomalies only allows more accurate depiction of relation between the two variables. In this case, much higher correlations are obtained, ranging from −0.87 in the upper 50 m to −0.95 in the 50–120 m layer, with no lag (0 months) for the upper and 37–42 month lag for the lower layer. While no lag in the upper 50 m can reflect simultaneous effects of summer ocean warming and sea ice melting, we note that the lower layer excludes the Chukchi and East Siberian shelves so a positive interannual lag is conceivable. Overall, this relation suggests that a large part of the variance in summertime ice thickness anomalies can potentially be explained by changes in the upper ocean heat content. However, more observations are needed from the evolving marginal ice zone in the Beaufort Sea to confirm this direct relationship between increased subsurface heat content and reduced sea ice thickness. On the modeling side, improvements are necessary toward eddy-resolving models able to accurately represent the magnitude of eddy-driven mass and heat transports and their impact on sea ice.

The overall correlations of heat content and ice thickness anomalies with AO and Pacific Decadal Oscillation (PDO) indices are quite low (below 0.2 for AO and below 0.3 for PDO). It is possible though that the increase of the upper ocean heat content and the associated thinning of sea ice in the western Arctic through the mid-1990s could be related to the combination of high PDO in the 1980s followed by the high AO through the mid-1990s. However, the warming and loss of sea ice during 1996–2004 is much harder to directly connect to the atmospheric forcing (Overland and Wang 2005) and, as such, points to the oceanic role in forcing the recent precipitous decline of sea ice in the western Arctic Ocean.

We finish this review with an analysis of recent freshwater accumulation in the Beaufort Gyre in response to warming climate and increased melt of sea ice. Freshwater content in the Arctic Ocean is usually calculated relative to a salinity of 34.8 for all water above the 34.8 isohaline (the salinity of incoming Atlantic Water through Fram Strait; Proshutinsky et al. 2009), and as such includes the waters of the halocline, formed by influx of Pacific origin water through Bering Strait and large amounts of freshwater from Eurasian and North American rivers. Anticyclonic wind forcing from the Beaufort high pressure system over the Canada Basin then leads to accumulation of the fresh Arctic surface waters via Ekman convergence and transport (Proshutinsky et al. 2009), promoting increased stratification (McLaughlin and Carmack 2010) and enhanced circulation of the anticyclonic Beaufort Gyre. While Ekman convergence is a local phenomenon, the overall accumulation of freshwater in the Beaufort Gyre is thought to be a result of Ekman transport at its periphery (large scale Ekman convergence), thus the freshwater for the Beaufort Gyre can be drawn from elsewhere in the Arctic. However, as discussed earlier, water derived from local ice melt combined with a stronger gyre circulation (e.g. Shimada et al. 2006) might be an increasingly important source of freshwater.

Figure 5.13 shows the summer freshwater content in the Beaufort Gyre from 2003 to 2010. Overall, strong anticyclonic forcing has led to a monotonic increase of the total freshwater content with by far the largest increase occurring in the winter between the 2007 and 2008 surveys when the Beaufort High was exceptionally strong.
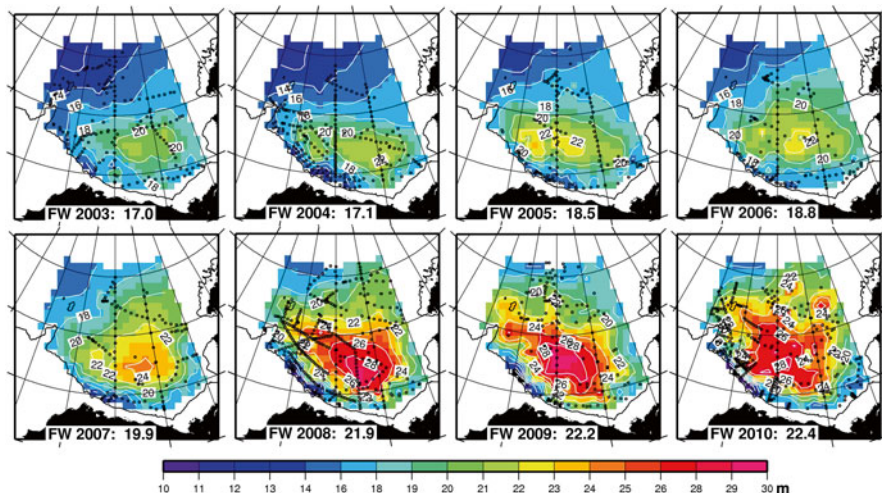
Fig. 5.13 Freshwater content in meters for the Beaufort Gyre region relative to a salinity of 34.8 psu from 2003 to 2010. The numbers at the *bottom* of each plot are the average over the area gridded and show the overall change from year to year. The largest change occurred during the winter between the 2007 and 2008 (Figure courtesy of Rick Krishfield, WHOI.)

The increase in freshwater also occurred during a time period of rapid summer ice retreat and ice melt; large amounts of thick, multi-year ice from the Canadian Arctic Archipelago melted in the southern Canada Basin and extensive summer sea ice retreat occurred in the western Beaufort and over the Northwind Ridge. Additional sources may also include reduced salt or increased freshwater fluxes through Bering Strait.

5.8   Summary

In this chapter, we presented an overview of the model-based mean regional ocean circulation in the Pacific-Arctic region, with emphasis on volume and heat transports into the western Arctic and their impact on sea ice. In particular, we discussed spatial and temporal variability of ocean currents and critical processes controlling northward flow of water. Model analyses and historical observations suggest that mesoscale eddies and meanders are dominant drivers controlling transport and variability of the Alaskan Stream, as well as mass and property fluxes across both the central and eastern Aleutian Island Passes and the western Aleutian Island Passes, between the Western Subarctic Gyre and the deep Bering Sea. Tidal mixing and rectification are also important, especially in shallow passes and on shelves; however their relative role is yet to be determined with eddy- and tide-resolving models. We made a compelling case for multi-year continuous and high spatio-temporal

observations in the western passes to validate and constrain modeled estimates of the long-term mean and variability of mass transports. Mesoscale eddies appear to be also important in shelf-basin exchanges, ice-ocean interactions and the expansion of the marginal ice zone (MIZ) in the Bering, Chukchi and Beaufort seas.

In addition, we argue for a number of particular model improvements to advance the realism and skill of simulation in the Pacific-Arctic region, consistent with the pan-Arctic advancements discussed by Maslowski et al. (2012). In particular, we discuss the importance of resolving eddies, tides and air-ice-ocean interactions. Higher horizontal and vertical resolution is required to address some of the present model limitations in representing small scale processes, such as mesoscale eddies, coastal and boundary currents or surface and bottom mixed layers, and to more realistically represent shelf and slope bathymetry, submarine canyons and narrow passes. Spatial resolution sufficient to resolve eddies and mixed layer processes will also likely improve our ability to estimate the on-shelf transport of nutrient-rich, deep Bering Sea water along the Bering Sea slope, which is important for downstream ecosystems throughout the northern Bering, Chukchi, and Beaufort seas. Future ecosystem, biogeochemistry and physical models will also need to be eddy-resolving to simulate small scale processes and quantify their impacts on Arctic-wide budgets of heat, freshwater, nutrients, and carbon.

Based on our model results and limited observations, we found that heat content of the Western Arctic ocean in the top 120 m has been increasing since the late 1990s and appears to be contributing to the rapid sea ice decline there. Our model analysis implies that the advection of warm water from Bering Strait regulates the retreat of sea ice and contributes to the relatively high surface air-sea fluxes over the Chukchi shelf. Earlier ice melt in the Chukchi Sea allows increased absorption of solar radiation and warming of water over the shelf, before it is exported into the Beaufort Sea where it can further contribute to sea ice melt. Based on evidence from observations and from our model, we argue that not all the heat content in the western Arctic Ocean gets removed back to the atmosphere every year before freezing in fall and early winter. We hypothesize that instead the remaining heat above the halocline and below the mixed layer acts to reduce sea ice growth in winter and preconditions an earlier ice melt each year, which further increases heat content in the region, thus resulting in a positive feedback accelerating summer reduction of the sea ice cover. The presence and spreading of a subsurface heat source in the western Arctic Ocean and the large-scale sea ice drift of the Beaufort Gyre help explain why the sea ice has continued to decline most dramatically in that part of the Arctic Ocean, even when large-scale atmospheric conditions were not always most favorable to such a decline (i.e. when the Arctic Oscillation Index was neutral or extremely negative).

Finally, we show that freshwater content of the Western Arctic Ocean increased during the 2000s. The coincidence of the locations in freshwater accumulation and in maximum sea ice thickness anomaly in the Beaufort Sea suggest an increased local freshwater contribution due to ice melt and an intensified circulation within the Beaufort Gyre.

References

Aagaard K, Coachman LK, Carmack EC (1981) On the halocline of the Arctic Ocean. Deep-Sea Res 28:529–545

Ahlnäs K, Garrison GR (1984) Satellite and oceanographic observations of the warm coastal current in the Chukchi Sea. Arctic 37:244–254

Arsen'ev VS (1967) Currents and water masses of the Bering Sea, Nauka, Izdatel'stro (translated in 1968, Northwest Fish. Center, Seattle)

Bond NA, Overland JE, Turet P (1994) Spatial and temporal characteristics of the wind forcing of the Bering Sea. J Clim 7:1119–1130

Cavalieri DJ, Martin S (1994) The contributions of Alaskan, Siberian, and Canadian coastal polynyas to the cold halocline layer of the Arctic Ocean. J Geophys Res 99:18343–18362

Chapman DC, Gawarkiewicz G (1995) Offshore transport of dense shelf water in the presence of a submarine canyon. J Geophys Res 100:13373–13387

Chelton DB, deSzoeke RA, Schlax MG, Naggar KE, Siwertz N (1998) Geographical variability of the first baroclinic Rossby radius of deformation. J Phys Oceanogr 28:433–460

Clement JL, Maslowski W, Cooper L, Grebmeier J, Walczowski W (2005) Ocean circulation and exchanges through the northern Bering Sea—1979–2001 model results. Deep-Sea Res II 52:3509–3540

Clement Kinney J, Maslowski W (2008) Results of recent Pacific-Arctic ice-ocean modeling studies at the Naval Postgraduate School. Chin J Polar Sci 19(2):230–236

Clement Kinney J, Maslowski W (2012) On the oceanic communication between the Western Subarctic Gyre and the deep Bering Sea. Deep-Sea Res I 66: 11–25 http://dx.doi.org/10.1016/j.dsr.2012.04.001

Clement Kinney J, Maslowski W, Okkonen S (2009) On the processes controlling shelf-basin exchange and outer shelf dynamics in the Bering Sea. Deep-Sea Res II 56:1351–1362. doi:10.1016/j.dsr2.2008.10.023

Clement Kinney J, Maslowski W, Aksenov Y, de Cuevas B, Jakacki J, Nguyen A, Osinski R, Steele M, Woodgate RA, Zhang J (2014) Chapter 7: On the flow through Bering Strait: a synthesis of model results and observations. In: Grebmeier JM, Maslowski W (eds) The Pacific Arctic region: ecosystem status and trends in a rapidly changing environment. Springer, Dordrecht, pp 167–198

Coachman LK, Aagaard K, Tripp RB (1975) Bering Strait: the regional physical oceanography. University of Washington Press, Seattle

Cokelet ED, Stabeno PJ (1997) Mooring observations of the thermal structure, density stratification and currents in the southeast Bering Sea basin. J Geophys Res 102(C10):22947–22964

Cokelet ED, Schall ML, Dougherty DM (1996) ADCP-referenced geostrophic circulation in the Bering Sea Basin. J Phys Oceanogr 26:1113–1128

Crawford WR, Cherniawski JY, Forman MGG (2000) Multi-year meanders and eddies in the Alaskan Stream as observed by TOPEX/Poseidon altimeter. Geophys Res Lett 27(7):1025–1028

Danielson S, Weingartner T, Aagaard K, Zhang J, Woodgate R (2012a) Circulation on the central Bering Sea shelf, July 2008 to July 2010. J Geophys Res. doi:10.1029/2012JC008303

Danielson S, Hedstrom K, Aagaard K, Weingartner T, Curchitser E (2012b) Wind-induced reorganization of the Bering shelf circulation. Geophys Res Lett. doi:10.1029/2012GL051231

Favorite F (1974) Flow into the Bering Sea through Aleutian Island passes. In: Hood DW, Kelley EJ (eds) Oceanography of the Bering Sea. University of Alaska, Fairbanks

Foreman MGG, Cummins PF, Cherniawsky JY, Stabeno PJ (2006) Tidal energy in the Bering Sea. J Mar Res 64(6):797–818. doi:10.1357/002224006779698341

Goosse H, Campin JM, Fichefet T, Deleersnijder E (1997) Sensitivity of a global ice–ocean model to the Bering Strait throughflow. Clim Dyn 13(5):349–358

Grebmeier JM, Dunton KH (2000) Benthic processes in the northern Bering/Chukchi seas: status and global change. In: Huntington HP (ed) Impacts of changes in sea-ice and other environmental parameters in the Arctic. Report of the Marine Mammal Commission Workshop, 15–17 Feb 2000, Girdwood, Alaska

Grebmeier JM, McRoy CP, Feder HM (1988) Pelagic-benthic coupling on the shelf of the northern Bering and Chukchi seas. I. Food supply source and benthic biomass. Mar Ecol Prog Ser 48:57–67

Hermann AJ, Stabeno PJ, Haidvogel DB, Musgrave DL (2002) A regional tidal/subtidal circulation model of the southeastern Bering Sea: development, sensitivity analyses and hindcasting. Deep-Sea Res II 49:5945–5967

Hogg AM, Killworth PD, Blundell JR, Dewar WK (2005) Mechanisms of decadal variability of the wind-driven ocean circulation. J Phys Oceanogr 35:512–531

Holloway G, Sou T (2002) Has Arctic Sea ice rapidly thinned? J Clim 15:1691–1701

Holloway G et al (2007) Water properties and circulation in Arctic Ocean models. J Geophys Res 112:C04S03. doi:10.1029/2006JC003642

Hughes FW, Coachman LK, Aagaard K (1974) Circulation, transport and water exchange in the western Bering Sea. In: Hood DW, Kelley EJ (eds) Oceanography of the Bering Sea. University of Alaska, Fairbanks

Hurlburt H, Wallcraft A, Schmitz W, Hogan P, Metzger E (1996) Dynamics of the Kuroshio/Oyashio current system using eddy-resolving models of the North Pacific Ocean. J Geophys Res 101(C1):941–976. doi:10.1029/95JC01674

Jackson JM, Allen SE, McLaughlin FA, Woodgate RA, Carmack EC (2011) Changes to the near-surface waters in the Canada Basin, Arctic Ocean from 1993–2009: a basin in transition. J Geophys Res 116:C10008. doi:10.1029/2011JC007069

Jackson JM, Williams WJ, Carmack EC (2012) Winter sea-ice melt in the Canada Basin, Arctic Ocean. Geophys Res Lett 39:L03603. doi:10.1029/2011GL050219

Kinder TH, Schumacher JD, Hansen DV (1980) Observations of a baroclinic eddy: an example of mesoscale variability in the Bering Sea. J Phys Oceanogr 10:1228–1245

Kowalik Z (1999) Bering Sea tides. In: Loughlin TR, Ohtani K (eds) Dynamics of the Bering Sea. University of Alaska Sea Grant, Fairbanks

Ladd C, Thompson L (2002) Decadal variability of North Pacific central mode water. J Phys Oceanogr 32:2870–2881

Maslowski W, Walczowski W (2002) Circulation of the Baltic Sea and its connection to the Pan-Arctic region – a large scale and high-resolution modeling approach. Boreal Environ Res 7(4):319–325

Maslowski W, Newton B, Schlosser P, Semtner AJ, Martinson DG (2000) Modeling recent climate variability in the Arctic Ocean. Geophys Res Lett 27(22):3743–3746

Maslowski W, Marble D, Walczowski W, Schauer U, Clement JL, Semtner AJ (2004) On climatological mass, heat, and salt transports through the Barents Sea and Fram Strait from a pan-Arctic coupled ice-ocean model simulation. J Geophys Res 109:C03032. doi:10.1029/2001JC001039

Maslowski W, Roman R, Clement Kinney J (2008a) Effects of mesoscale eddies on the flow of the Alaskan Stream. J Geophys Res 113:C07036. doi:10.1029/2007JC004341

Maslowski W, Clement Kinney J, Marble DC, Jakacki J (2008b) Towards eddy-resolving models of the Arctic Ocean. In: Hecht MW, Hasumi H (eds) Ocean modeling in an eddying regime, vol 177, Geophysics monograph series. American Geophysical Union, Washington, DC

Maslowski W, Clement Kinney J, Higgins Roberts AF (2012) The future of Arctic Sea ice. Annu Rev Earth Planet Sci 40:625–654

McClean JL, Maslowski W, Maltrud M (2001) Towards a coupled environmental prediction system. In: Alexandrov VN, Dongorra JJ, Juliano BA, Renner RS, Tan CJK (eds) Computational science – ICCS 2001, Lecture notes in computer science 2073. Springer, Berlin

McLaughlin FA, Carmack EC (2010) Deepening of the nutricline and the chlorophyll maximum in the Canada Basin interior, 2003–2009. Geophys Res Lett 37:L24602. doi:10.1029/2010GL045459

Münchow A, Carmack EC (1997) Synoptic flow and density observations near an Arctic shelf break. J Phys Oceanogr 27:1402–1419

Musgrave DL, Weingartner TJ, Royer TC (1992) Circulation and hydrography in the northwestern Gulf of Alaska. Deep-Sea Res 39:1499–1519

Newton R, Schlosser P, Martinson DG, Maslowski W (2008) Freshwater distribution in the Arctic Ocean: simulation with a high-resolution model and model-data comparison. J Geophys Res 113:C05024. doi:10.1029/2007JC004111

Nikolopoulos A, Pickart RS, Fratantoni PS, Shimada K, Torres DJ, Jones EP (2009) The western Arctic boundary current at 152°W: structure, variability, and transport. Deep-Sea Res II 56:1164–1181

Ohtani K (1970) Relative transport in the Alaskan Stream in winter. J Oceanogr Soc Jpn 26:271–282

Okkonen SR (1992) The shedding of an anticyclonic eddy from the Alaskan Stream as observed by the GEOSAT altimeter. Geophys Res Lett 19(24):2397–2400

Okkonen SR (1993) Observations of topographic planetary waves in the Bering Slope Current using GEOSAT altimeter. J Geophys Res 98(12):22603–22613

Okkonen SR (1996) The influence of an Alaskan Stream eddy on flow through Amchitka Pass. J Geophys Res 101(C4):8839–8851

Okkonen SR, Jacobs GA, Metzger EJ, Hurlburt HE, Shriver JF (2001) Mesoscale variability in the boundary currents of the Alaska Gyre. Cont Shelf Res 21:1219–1236

Okkonen SR, Ashjian CJ, Campbell RG, Maslowski W, Clement-Kinney JL, Potter R (2009) Intrusion of warm Bering/Chukchi waters onto the shelf in the western Beaufort Sea. J Geophys Res 114:C00A11. doi:10.1029/2008JC004870

Onishi H (2001) Spatial and temporal variability in a vertical section across the Alaskan Stream and Subarctic Current. J Oceanogr 57:79–91

Onishi H, Ohtani K (1999) On seasonal and year to year variation in flow of the Alaskan Stream in the central North Pacific. J Oceanogr 55:597–608

Overland JE, Roach AT (1987) Northward flow in the Bering and Chukchi seas. J Geophys Res 92:7097–7105

Overland JE, Wang M (2005) The Arctic climate paradox: the recent decrease of the Arctic Oscillation. Geophys Res Lett 32(6):L06701. doi:10.1029/2004GL021752

Overland JE, Spillane MC, Hurlburt HE, Wallcraft AJ (1994) A numerical study of the circulation of the Bering Sea basin and exchange with the North Pacific Ocean. J Phys Oceanogr 24:736–758

Paluszkiewicz T, Niebauer HJ (1984) Satellite observations of circulation in the eastern Bering Sea. J Geophys Res 89:3663–3678

Panteleev GG, Stabeno P, Luchin VA, Nechaev DA, Ikeda M (2006) Summer transport estimates of the Kamchatka Current derived as a variational inverse of hydrophysical and surface drifter data. Geophys Res Lett 33:L09609. doi:10.1029/2005GL024974

Paquette R, Bourke R (1974) Observations on the coastal current of arctic Alaska. J Mar Res 32:195–207

Perovich DK, Richter-Menge JA, Jones KF, Light B (2008) Sunlight, water, and ice: extreme Arctic sea ice melt during the summer of 2007. Geophys Res Lett 35:L11501. doi:10.1029/2008GL034007

Pickart RS, Weingartner TJ, Zimmermann S, Torres DJ, Pratt LJ (2005) Flow of winter-transformed water into the Western Arctic. Deep-Sea Res II 52:3175–3198

Polyakov IV et al (2010) Arctic Ocean warming contributes to reduced polar ice cap. J Phys Oceanogr 40:2743–2756

Proshutinsky A, Ashik I, Häkkinen S, Hunke E, Krishfield R, Maltrud M, Maslowski W, Zhang J (2007) Sea level variability in the Arctic Ocean from AOMIP models. J Geophys Res 112:C04S08. doi:10.1029/2006JC003916

Proshutinsky A, Krishfield R, Timmermans M-L, Toole J, Carmack E, McLaughlin F, Williams WJ, Zimmermann S, Itoh M, Shimada K (2009) Beaufort Gyre freshwater reservoir: state and variability from observations. J Geophys Res 114: C00A10. http://dx.doi.org/10.1029/2008JC005104

Reed RK (1984) Flow of the Alaskan Stream and its variations. Deep-Sea Res 31(4):369–386

Reed RK (1990) A year-long observation of water exchange between the North Pacific and the Bering Sea. Limnol Oceanogr 35:1604–1609

Reed RK, Stabeno PJ (1989) Circulation and property distributions in the Central Bering Sea, Spring 1988, NOAA technical report, ERL 439-PMEL 39, NTIS PB90–155847, 13 pp

Reed RK, Stabeno PJ (1993) The recent return of the Alaskan Stream to Near Strait. J Mar Res 51:515–527

Reed RK, Stabeno PJ (1997) Long-term measurements of flow near the Aleutian Islands. J Mar Res 55:565–575

Reed RK, Stabeno PJ (1999) The Aleutian North Slope current. In: Loughlin TR, Ohtani K (eds) Dynamics of the Bering Sea: a summary of physical, chemical, and biological characteristics, and a synopsis of research on the Bering Sea, North Pacific Marine Science Organization (PICES), University of Alaska Sea Grant, AK-SG-99-03

Reed RK, Taylor NE (1965) Some measurements of the Alaska Stream with parachute drogues. Deep-Sea Res 12:777–784

Reed RK, Khen GV, Stabeno PJ, Verkhunov AV (1993) Water properties and flow over the deep Bering Sea basin, summer 1991. Deep-Sea Res 40:2325–2334

Roach AT, Aagaard K, Pease CH, Salo SA, Weingartner T, Pavlov V, Kulakov M (1995) Direct measurements of transport and water properties through the Bering Strait. J Geophys Res 100:18443–18457

Roden GI (1995) Aleutian Basin of the Bering Sea: thermohaline, oxygen, nutrient, and current structure in July 1993. J Geophys Res 100:13539–13554

Royer TC, Emery WJ (1987) Circulation in the Gulf of Alaska, in 1981. Deep-Sea Res 34:1361–1377

Rudels B, Jones EP, Anderson LG, Kattner G (1994) On the intermediate depth waters of the Arctic Ocean. In: Johannesen OM, Muench RD, Overland JE (eds) The polar oceans and their role in shaping the global environment: the Nansen centennial volume. American Geophysical Union, Washington, DC

Schauer U, Beszczynska-Möller A, Walczowski W, Fahrbach E, Piechura J, Hansen E et al (2008) Variation of measured heat flow through the Fram Strait between 1997 and 2006. In: Dickson RR (ed) Arctic-subarctic ocean fluxes: defining the role of the northern seas in climate. Springer Science + Business Media B.V., Dordrecht

Schumacher JD, Reed RK (1992) Characteristics of currents over the continental slope of the eastern Bering Sea. J Geophys Res 97:9423–9433

Shimada K, Carmack E, Hatakeyama K, Takizawa T (2001) Varieties of shallow temperature maximum waters in the Western Canadian Basin of the Arctic Ocean. Geophys Res Lett 28:3441–3444

Shimada K, Kamoshida T, Itoh M, Nishino S, Carmack E, McLaughlin F, Zimmermann S, Proshutinsky A (2006) Pacific Ocean inflow: influence on catastrophic reduction of sea ice cover in the Arctic Ocean. Geophys Res Lett 33:L08605. doi:10.1029/2005GL025624

Solomon H, Ahlnäs K (1978) Eddies in the Kamchatka Current. Deep-Sea Res 25:403–410

Spall MA (2007) Circulation and water mass transformation in a model of the Chukchi Sea. J Geophys Res 112:C05025. doi:10.1029/2005JC002264

Spall MA, Pickart RS, Fratantoni P, Plueddemann A (2008) Western Arctic shelfbreak eddies: formation and transport. J Phys Oceanogr 38:1644–1668

Springer AM, McRoy CP (1993) The paradox of pelagic food webs in the northern Bering Sea. III. Patterns of primary production. Cont Shelf Res 13:575–599

Stabeno PJ, Hermann AJ (1996) An eddy resolving model of circulation on the western Gulf of Alaska shelf. II. Comparison of results to oceanic observations. J Geophys Res 101:1151–1161

Stabeno PJ, Reed RK (1992) A major circulation anomaly in the western Bering Sea. Geophys Res Lett 19:1671–1674

Stabeno PJ, Reed RK (1994) Circulation in the Bering Sea Basin observed by satellite-tracked drifters: 1986–1993. J Phys Oceanogr 24:848–854

Stabeno PJ, Schumacher JD, Ohtani K (1999) The physical oceanography of the Bering Sea. In: Loughlin TR, Ohtani K (eds) Dynamics of the Bering Sea: a summary of physical, chemical, and biological characteristics, and a synopsis of research on the Bering Sea, North Pacific Marine Science Organization (PICES), Univ. of Alaska Sea Grant, AK-SG-99-03

Stabeno PJ, Kachel DG, Kachel NB, Sullivan ME (2005) Observations from moorings in the Aleutian Passes: temperature, salinity and transport. Fish Oceanogr 14(1):39–54. doi:10.1111/j.1365-2419.2005.00362.x

Steele M, Morison J, Ermold W, Rigor I, Ortmeyer M, Shimada K (2004) Circulation of summer Pacific halocline water in the Arctic Ocean. J Geophys Res 109:C02027. doi:10.1029/2003JC002009

Stroeve JC, Maslanik J, Serreze MC, Rigor I, Meier W, Fowler C (2011) Sea ice response to an extreme negative phase of the Arctic Oscillation during winter 2009/2010. Geophys Res Lett 38:02502. doi:10.1029/2010GL045662

Sumata H, Shimada K (2007) Northward transport of pacific summer water along the Northwind Ridge in the Western Arctic Ocean. J Oceanogr 63:363–378

Thompson RE (1972) On the Alaskan Stream. J Phys Oceanogr 2:363–371

Verkhunov AV, Tkachenko YY (1992) Recent observations of variability in the western Bering Sea current system. J Geophys Res 97:14369–14376

Walsh JJ, Dieterle DA, Maslowski W, Whitledge TE (2004) Decadal shifts in biophysical forcing of marine food webs in the Arctic: numerical consequences. J Geophys Res 109:C05031. doi:10.1029/2003JC001945

Warren BA, Owens WB (1988) Deep currents in the central Subarctic Pacific Ocean. J Phys Oceanogr 18:529–551

Watanabe E (2011) Beaufort shelf break eddies and shelf-basin exchange of Pacific summer water in the western Arctic Ocean detected by satellite and modeling analyses. J Geophys Res 116:C08034. doi:10.1029/2010JC006259

Weingartner TJ, Cavalieri DJ, Aagaard K, Sasaki Y (1998) Circulation, dense water formation and outflow on the northeast Chukchi Sea shelf. J Geophys Res 103:7647–7662

Weingartner TJ, Danielson S, Sasaki Y, Pavlov V, Kulakov M (1999) The Siberian Coastal Current: a wind- and buoyancy-forced Arctic coastal current. J Geophys Res 104:29697–29713. doi:10.1029/1999JC900161

Weingartner T, Aagaard K, Woodgate R, Danielson S, Sasaki Y, Cavalieri D (2005) Circulation on the North Central Chukchi Sea Shelf. Deep-Sea Res II 52(24–26):3150–3174

Williams W, Shroyer E, Clement Kinney J, Itoh M, Maslowski W (2014) Chapter 6: Shelf-break exchange in the Bering, Chukchi and Beaufort seas. In: Grebmeier JM, Maslowski W (eds) The Pacific Arctic region: ecosystem status and trends in a rapidly changing environment. Springer, Dordrecht, pp 133–166

Winsor P, Chapman DC (2004) Pathways of Pacific water across the Chukchi Sea: a numerical model study. J Geophys Res 109:C03002. doi:10.1029/2003JC001962

Woodgate RA, Aagaard K, Muench RD, Gunn J, Björk G, Rudels B, Roach AT, Schauer U (2001) The Arctic Ocean Boundary Current along the Eurasian slope and the adjacent Lomonosov Ridge: water mass properties, transports and transformations from moored instruments. Deep-Sea Res I 48(8):1757–1792

Woodgate RA, Aagaard K, Weingartner TJ (2005) A year in the physical oceanography of the Chukchi Sea: moored measurements from autumn 1990–1991. Deep-Sea Res II 52:3116–3149. doi:10.1016/j.dsr2.2005.10.016

Xie S-P, Kunitani T, Kubokawa A, Nonaka M, Hosoda S (2000) Interdecadal thermocline variability in the North Pacific for 1958–97: a GCM simulation. J Phys Oceanogr 30:2798–2813

Zhang Y, Maslowski W, Semtner A (1999) Impact of mesoscale ocean currents on sea ice in high-resolution Arctic ice and ocean simulations. J Geophys Res 104(C8):18409–18429. doi:10.1029/1999JC900158